Dalton Transactions

Accepted Manuscript

ROYAL SOCIETY OF CHEMISTRY

rsc.li/dalton

View Article Online
DOI: 10.1039/C6DT03519A

Dalton Transactions

ARTICLE

Evaluation of functionalized mesoporous silica SBA-15 as a carrier system for $Ph_3Sn(CH_2)_3OH$ against A2780 ovarian carcinoma cell line

Received 00th January 20xx,
Accepted 00th January 20xx

DOI: 10.1039/x0xx00000x

www.rsc.org/

Christian Bensing,[#a] Marija Mojić,[#b] Santiago Gómez-Ruiz,[*c] Sandra Carralero,[c] Biljana Dojčinović,[d] Danijela Maksimović-Ivanić,[b] Sanja Mijatović[b] and Goran N. Kaluđerović[*e]

SBA-15|Sn3, a mesoporous silica-based material (derivative of SBA-15) loaded with organotin compound $Ph_3Sn(CH_2)_3OH$ (Sn3), possess improved antitumor potential against A2780 high-grade serous ovarian carcinoma cell line in comparison to Sn3. It is demonstrated that both the compound and the nanostructured material are internalized by A2780 cells. Similar mode of action of Sn3 and SBA-15|Sn3 against A2780 cell line was found. Explicitly, induction of apoptosis, caspase 2, 3, 8 and 9 activation, accumulation of cells in hypodiploid phase as well as accumulation of ROS was observed. Interestingly, Sn3 loaded in mesoporous silica-based material needed to reach concentration 3.5 times lower than the IC_{50} value of Sn3 compound, pointing out on higher effect of the SBA-15|Sn3 than Sn3 alone. Clonogenic potential, growth in 3D culture as well as mobility of cells were disturbed in the presence of SBA-15|Sn3. Such behavior could be associated with the suppression of p-38 MAPK. Less profound effect of Sn3 comparing to SBA-15|Sn3 could be attributed to a different regulation of p-38 and STAT-3 which are mainly responsible for appropriate cellular response to diverse stimuli or metastatic properties.

Introduction

One of the most interesting fields of the modern nanomedicine is related to nanoparticles efficient in hosting, protecting, carrying and releasing therapeutic agents at target tissues.[1–3] 2001. mesoporous silica nanoparticles (MSNs) were suggested, by the group of M. Vallet-Regi, as an interesting drug release system.[4] Since then many researchers showed a growing interest in MSNs for their innovative potential in nanomedicine.[1] MSNs can be prepared in various sizes and shapes, survive in severe milieu and have various regular pore sizes.[5] Furthermore, the pore diameter can be altered to preserve diverse substances (2–50 nm) enabling their transportation.[6] Such pores can adopt various biomaterials of different nature, from small molecules to proteins, among others, in relatively large amounts.[7,8]

MSNs and other silica-based materials, non-toxic to cells,[9] are assumed as extraordinary particles in quite a few fields of medicine such as bone regeneration, for example, however, in cancer treatment not many investigations have been reported until now.[10–13] An interesting property of this kind of materials is that they favourably accumulate in solid tumours due to the increased permeation and retention effect.[14,15]

From our pioneering work, which began 2009, it is revealed that MSNs and other silica-based materials such as SBA-15 and MCM-41 do not affect tumor cell lines in high concentrations, up to 1 mg/mL.[16–18] On the contrary, the same kind of materials loaded with titanocene compounds enhance the cytotoxicity in tumor cells, depending on the particle type (SBA-15 or MCM-41), titanium(IV) complex as well as its loaded amount. Moreover, SBA-15 was found to be superior to MCM-41 as carrier system. Recently, we reported on SBA-15 derivative loaded with $Ph_3Sn(CH_2)_6OH$ observing that this material was ca. 150 time more active than SBA-15 loaded with titanium(IV) complexes.[19] The strong therapeutic potential of organotin(IV)-loaded mesoporous silica lies in the development of a nonproliferative melanocyte-like phenotype of surviving cells. Thus, this nonaggressive suppression of tumor growth with nontoxic doses of the drug, much lower than the IC_{50} concentration of $Ph_3Sn(CH_2)_6OH$, is highly efficient against melanoma cells. Contrarily

[a] Institute of Chemistry, Martin Luther University Halle-Wittenberg, Kurt-Mothes-Straße 2, D-06120 Halle, Germany
[b] Institute for Biological Research "Sinisa Stankovic" University of Belgrade, Bulevar despota Stefana 142, 11060 Belgrade, Serbia
[c] Departamento de Biología y Geología, Física y Química Inorgánica, E.S.C.E.T., Universidad Rey Juan Carlos, 28933 Móstoles, Madrid, Spain
[d] Department of Chemistry, Institute of Chemistry, Tehnology and Metallurgy, University of Belgrade, Studentski trg 12-14, 11000 Belgrade, Serbia.
[e] Department of Bioorganic Chemistry, Leibniz-Institute of Plant Biochemistry, Weinberg 3, D 06120 Halle (Saale), Germany
* Correspondence: Goran N. Kaluđerović, phone: +49 345 5582 1370, Fax: +49 345 5582 1309, E-mail: goran.kaluderovic@ipb-halle.de; Santiago Gómez-Ruiz, phone: +34 914 888 507, Fax: ++34 914 888 500, E-mail: santiago.gomez@urjc.es.

# equally contributed
† Electronic Supplementary Information (ESI) available: ^{29}Si MAS, ^{13}C CP/MAS and ^{119}Sn MAS NMR spectra, XRD diffractogram, N_2-adsorption-desorption isotherm, particle size distribution determined, pore diameter distribution for of SBA-15|Sn3, Sn3 release study from SBA-15|Sn3

to the induction of apoptosis as the most employed conventional approach in oncotherapy, this mode of action has numerous advantages.[20] One of them is avoiding of compensatory proliferation phenomenon present in tumors in response to cell death in the neighborhood.[21]

As one of the most lethal gynecological malignancy and fifth leading cause of death in women,[21] ovarian cancer cause more than 100,000 instances worldwide each year.[22] From the epithelial ovarian cancer, four major histological subtypes are identified.[23] Namely, serous, endometrioid, clear cell and mucinous carcinoma from which serous type is responsible for ca. 70 % of epithelial ovarian cancers. Furthermore, high-grade serous ovarian carcinoma (HGSOC) is considered as the most aggressive subtype causing around 70 % of all ovarian cancer deaths.[25] A2780 cell line belongs to the most prevalent subtype of HGSOC, beside CAOV3, SK-OV-3, IGROV1 and OVCAR-3 cells.[26] Most patients, after radical surgery and primary excessive response to platinum- and taxane-based chemotherapy, face a relapse of HSGOC with a survival of only 18 months.[25] As a consequence, development of novel drugs is of high importance in order to advance current therapies.

Herein we report the preparation and characterization of the organotin(IV) compound $Ph_3Sn(CH_2)_3OH$ (Sn3) which has been grafted into functionalized SBA-15 (→SBA-15|Sn3). Furthermore, Sn3 and SBA-15|Sn3 have been tested against A2780, A549 and DLD-1 tumor cell lines. A2780, as model of HGSOC,[23] was chosen for evaluation of Sn3 and SBA-15|Sn3 mechanism of action. This cell line overexpressed multidrug resistant pumps and therefore is an ideal model system for assessment of acquired resistance to chemotherapeutics drugs.[27] It is well known that metal-based drugs belong to the group of the most sensitive compounds for efflux by the pumps.[28] On the other side, compounds loaded in MSNs and other silica-based materials accumulate into the cells due to down regulation of transporters as well as bypass the efflux action by MSN themselves.[29] Therefore, it was of interest to compare the effectiveness and the mechanism of action of $Ph_3Sn(CH_2)_3OH$ (Sn3) compound in free and loaded, SBA-15|Sn3, form. Thus, the influence on the cell death, metastatic properties of the cell and intracellular response were estimated.

Experimental

Materials and methods

All manipulations for the synthesis of tin compound and the functionalized materials were performed under dry nitrogen gas using standard Schlenk techniques and glove box. Solvents were distilled from the appropriate drying agents and degassed before use. 3-chloropropyltriethoxysilane (CPTS) was purchased from Sigma-Aldrich and used directly without further purification.

^{1}H, ^{13}C and ^{119}Sn NMR spectra for Sn3 were recorded on Varian Gemini 400 and ^{13}C CP/MAS NMR, ^{29}Si MAS NMR and ^{119}Sn MAS NMR spectra were recorded on a Varian-Infinity Plus Spectrometer at 400 MHz. ^{13}C CP/MAS NMR (4.40 µs 90º pulse, spinning speed of 6 MHz, pulse delay 2 s), ^{29}Si MAS NMR (8 µs 90º pda, spinning speed of 6 MHz, pulse delay 10 s) ^{119}Sn MAS NMR (8 µs 90º pda, spinning speed of 6 MHz, pulse delay 10 s) and X-ray diffraction (XRD) pattern of the silicas were obtained on a Phillips Diffractometer model PW3040/00 X'Pert MPD/MRD at 45 KV and 40 mA, using a wavelength Cu Kα (λ = 1.5418 Å). MS (ESI) spectra were taken on a Finnigan MAT TSQ 7000 (voltage 4.5 kV, sheath gas nitrogen) instrument. C, H and N elemental microanalyses were carried out with a CHNS-932 (LECO) elemental analyzer (Sn3), in the Microanalytical Laboratory of the University of Halle. N_2 gas adsorption-desorption isotherms were performed using a Micromeritics ASAP 2020 analyzer. Scanning electron micrographs and morphological analysis were carried out on a XL30 ESEM Phillips with an energy dispersive spectrometry system (EDS). The samples were treated with a sputtering method with the following parameters: Sputter time 100 s, Sputter current 30 mA, film thickness 20 nm using a Sputter coater BAL-TEC SCD 005. Conventional transmission electron microscopy (TEM) was carried out on a TECNAI 20 Phillips, operating at 200 kV. SBA-15 and SBA-15p (Table 1) were prepared as described previously.[19]

Synthesis of $Ph_3Sn(CH_2)_3OH$ (Sn3)

Ph_3SnH (5.86 g, 16.7 mmol), allylalcohol (2.8 mL, 33.4 mmol) and AIBN (0.14 mg, 0.8 mmol) were stirred for 3 h at 80 °C.[30] Precipitated product was collected, dried under vacuum and subsequently two times recrystallized from petrol ether. Mother liquor was concentrated and purified by column chromatography (eluent: petrol ether:$CHCl_3$ = 2:1, afterwards ether) and recrystallized from *n*-hexane. Yield: 4.43 g (64.9%); colorless needles; MP: 104–105 °C; MS (ESI): *m/z* = calc. $[C_{21}H_{22}OSn\ –H^+]^-$ 410.1, found: 409.4; Elemental analysis (in %): calc. for $C_{21}H_{22}OSn$: C 61.65, H 5.42, found: C 61.57, H 5.27; ^{1}H NMR ($CDCl_3$, 400 MHz): δ (in ppm) = 1.26 (t, ^3J(H,H) = 5.48 Hz, 1H; O*H*), 1.49–1.55 (m, 2H; C$^1H_2$), 1.98 (m, 2H; C$^2H_2$), 3.65 (m, 2H; C$^3H_2$), 7.37 (m, 9H; Ar-H_m und Ar-H_p), 7.56 (m, 6H; Ar-H_o); ^{13}C NMR ($CDCl_3$, 101 MHz): δ (in ppm) = 6.7 (C^1, ^1J(^{119}Sn,C) = 397.1 Hz), 29.3 (C^2, ^2J($^{117/119}$Sn,C) = 21.2 Hz), 65.6 (C^3, ^3J(^{119}Sn,C) = 66.3 Hz), 128.5 (C_m, ^3J(^{119}Sn,C) = 48.8 Hz), 128.9 (C_p, ^4J($^{117/119}$Sn,C) = 11.0 Hz), 137.0 (C_o, ^2J(^{119}Sn,C) = 36.1 Hz), 138.9 (C_i, ^1J(^{119}Sn,C) = 491.6 Hz).; ^{119}Sn NMR ($CDCl_3$, 149 MHz): δ (in ppm) = –99.3 (s, Ph_3Sn).

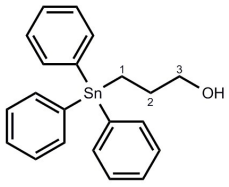

Preparation of SBA-15|Sn3

A solution of 3-(triphenylstannyl)propan-1-ol (0.315 g, 0.77 mmol) in toluene (100 mL) was added to SBA-15p (1.00 g). Subsequently, triethylamine (75 mg, 0.92 mmol) was added and the mixture was stirred 48 h at 80 ºC. The slurry was filtered through a frit and the solid residue washed with toluene (3 × 30 mL), hexane (3 × 30 mL), water:ethanol (1:1, 2 × 20 mL) and diethylether (2 × 60 mL). The resultant solid was dried under vacuum at room temperature for 24 h to give a white free flowing powder. ^{29}Si MAS NMR: δ (in ppm) = –113

View Article Online
DOI: 10.1039/C6DT03519A

(br, s; including Q4 [$Si(OSi)_2(OH)$], Q3 [$Si(OSi)_2(OH)$], Q2 [$Si(OSi)_2(OH)_2$]), –73 to –62 (br, [$SiO–Si(OEt)_n(CH_2CH_2CH_2Cl)$]; *n* = 0–1). ^{13}C CP/MAS NMR: δ (in ppm) = 4.3 (CH_2–Sn and CH_2–Si), 11.4 (CH_2 of CPTS), 18.1 and 31.2 (CH_2 of Sn-containing fragment), 24.6 (CH_3 of Et), 45.0 (O–CH_2 of Et), 51.7 (O–CH_2 of Sn-containing fragment), 126.7 and 134.5 (Ph); ^{119}Sn MAS NMR: δ (in ppm) = –105 ppm. %Sn (obtained by X-ray fluorescence) = 4.35%. Textural parameters of the synthesized surface obtained by N_2-adsorption-desorption isotherms: BET-surface: 417 $m^2 \cdot g^{-1}$, pore volume: 0.49 $cm^3 \cdot g^{-1}$, pore size: 4.88 nm and wall thickness: 5.82 nm.

Table 1 Textural and chemical properties of synthesized materials SBA-15, SBA-15p and SBA-15|Sn3 calculated from N_2-adsorption-desorption isotherms, XRD and XRF analysis

Surface	d_{100} [nm]	a_0 [nm]	S_{BET} [m^2/g]	V_m [cm^3/g]	D_P [nm]	W_d [nm]
SBA-15	9.22	10.65	932	0.94	4.97	5.68
SBA-15p	9.48	10.91	535	0.58	4.88	6.03
SBA-15|Sn	9.27	10.70	417	0.49	4.88	5.82

Reagents and cells

Fetal calf serum (FCS), RPMI-1640, phosphate-buffered saline **(**PBS), dimethyl sulfoxide (DMSO), Sulforhodamine (SRB), crystal violet (CV) and propidium iodide (PI) were obtained from Sigma (St. Louis, MO). Annexin V-FITC (AnnV) was from Santa Cruz Biotechnology (Dallas, TX). Human ovarian A2780 cell line was a kind gift from Thomas Miller (Institute for Oncology, Martin Luther University Halle-Wittenberg. Matrigel™ Basement Membrane Matrix was purchased from BD Biosciences. Cells were regularly propagated in HEPES-buffered RPMI-1640 medium supplemented with 10% FCS, 2 mM L-glutamine, 0.01% sodium pyruvate and antibiotics (culture medium) at 37 °C in a humidified atmosphere with 5% CO_2. Cells were seeded at 5 × 10^3 cells/well in 96-well plates for viability determination and 2.5 × 10^5 cells/well in 6-well plates for flow cytometry.

Preparation of drug solutions

Sn3 was dissolved in DMSO at 20 mM and kept at –20 °C until use. SBA-15|Sn3 stock (1 mg/mL) was dissolved in culture medium directly before use. Immediately before treatment various working solutions were prepared in culture medium.

Sulforhodamine test (SRB)

A2780 cells were seeded at 1,000 cells/well density and treated with wide range of doses of Sn3 or SBA-15|Sn3 for 72 h. At the end of cultivation SRB test was done exactly as described.[31]

Morphological analysis (AO/EB double staining)

Sn3 or SBA-15|Sn3 induced cell death in A2780 ovarian tumor cells was determined using acridine orange (AO) and ethidium bromide (EB), double staining according to standard procedures and examined under a fluorescence microscope.[33] A2780 cells were seeded overnight on 8 chamber slides (6,000 cells/chamber) in 400 µL of complete medium. The next day, cells were treated with 2×IC_{50} or 2×MC_{50} of Sn3 or SBA-15|Sn3 respectively, for 24 h. After this period, cells on the slides were stained with acridine orange/ethidium bromide mixture (3 µg/mL AO and 10 µg/mL EB in PBS), and visualized under a fluorescence microscope (Carl Zeiss).

Caspase 2, 3, 8 and 9 enzyme activity assays

Activity of caspases 2, 3, 8 and 9 was measured using the caspase substrate cleavage assay. A2780 cells were seeded at density of 1×10^6/well in 6 well plate. After exposure to IC_{50} or MC_{50} concentration of Sn3 or SBA-15|Sn3, cells were sampled after 2 h for cleavage of caspases. Adherent cells were washed with cold PBS, collected with a cell scraper, and suspended in cell lyses buffer (50 mM Hepes pH 7.4, 1% Triton X100, all from Sigma-Aldrich). After incubation for 10 min on ice and centrifugation, protein concentrations of the supernatants were measured according to a method of Bradford (Bio-Rad Laboratories). Samples (50 µg protein extract) were incubated on a microplate at 37 °C overnight in reaction buffer (50 mM Hepes pH 7.4, 0.1% CHAPS, 5 mM EGTA, 5% glycerol) containing 10 mM DTT (all from Sigma-Aldrich) and a specific substrate of caspases. Extinction of released *p*-nitroaniline was measured at 405 nm using a 96 well plate reader (Tecan Spectra) and activity of caspases 2, 3, 8 and 9 was evaluated by OD ratio of treated/untreated samples.[32,34]

ICP-MS analysis

For drug uptake experiments A2780 cells (1.2×10^6) were seeded in the flask. After 24 h cells were treated with IC_{50} or MC_{50} dose of Sn3, SBA-15|Sn3 or SBA-15p (10 mL) for 24 h. Afterwards the cells were washed with PBS (4 mL) and trypsinized (1 mL). Cells were resuspended in PBS (4 mL) and centrifuged (5000 U/min, 5 min). Cell pallet was washed two times with PBS (1 mL). Lyophilised cells was analysed with ICP-MS (Wessling Laboratorien GmbH, Oppin, Germany).

For Sn3 release study SBA-15|Sn3 (2.0 mg) was suspended in completed medium (1 mL), for each time point, and tin content was investigated with ICP-MS after 0.08, 2, 4, 6, 24 and 72 h, in triplicate. Explicitly, after soaking at 37 °C suspensions were centrifuged (5000 U/min) and supernatants were used for analysis. Liquid samples were diluted with purified water (1:100, v/v). The Thermo Scientific iCAP Qc ICP-MS instrument was optimized for optimum performance in standard mode using the supplied autotune protocols. The ICP-MS instrument was tuned using a solution TUNE B iCAP Q (1 µg/L of each: Ba, Bi, Ce, Co, In, Li, U) provided by the manufacturer Thermo Scientific, Germany. External standards for the instrument calibration were prepared on the basis of a tin plasma standard solution (Specpure®, Sn 100 µg/mL certified reference solution ICP Standard purchased from Alfa Aesar GmbH & Co KG, Germany). For extracts, the limit of quantitation (LOQ) for tin was determined to be 2.02 ng/L. The measurement was performed on isotope ^{120}Sn.

Cell cycle analysis

Cells were incubated with a IC_{50} or MC_{50} dose of Sn3 or SBA-15|Sn3 for 72 h and cell cycle analysis is done as previously described.[35]

Measurement of ROS

For detection of reactive oxygen species the redox-sensitive dye dihydrorhodamine 123 (DHR) was used. The cells were stained with 1 mM DHR for 20 min before treatment with an IC_{50} or MC_{50} dose of Sn3 or SBA-15|Sn3. After 48 h cells were trypsinized, washed in PBS, and the fluorescence intensity was analysed with a CyFlow® Space Partec using PartecFloMax® software (Partec GmbH, Münster, Germany).

Cell clonogenic survival assay

Cells were pretreated for 72 h with an IC_{50} or MC_{50} dose of Sn3 or SBA-15|Sn3, then detached, counted and 1000 cells/well were reseeded. Cells were grown for 5 days without changing the medium. After 9 days of cultivation, colonies were fixed with 4% PFA for 30 min at RT and then stained 30 min at RT with 0.25% 1,9-dimethyl methylene blue in 50% ethanol. Finally, colonies were washed twice with PBS and analyzed by light microscopy. Plate efficiency (PE)is calculated as number of colonies/number of cells×100, while surviving fraction is calculated as PE of treatment/PE of control×100.

Adhesion assay

96 well plates were covered with matrigel 10 µg/mL at 4 °C overnight. Wells were washed 3 times with PBS before seeding the cells. Cells were pretreated for 72 h with an IC_{50} or MC_{50} dose of Sn3 or SBA-15|Sn3, then detached, counted and left for approximately 30 min for membrane reconstitution. Then, 30,000 cells/well are allowed to adhere to matrigel for 1 h. Nonadherent cells were then washed 3 x with PBS, fixed with 4% PFA, stained with crystal violet 15 min at RT. Cells were washed with tap water, and dye was dissolved in 33 % of acetic acid. Absorbance was measured at 570 nm and results are calculated as percentage of control nontreated cells.

Transmigration assays

Cells were pretreated for 72 h with an IC_{50} or MC_{50} dose of Sn3 or SBA-15|Sn3, and then detached, counted and 2×10^5 cell were seeded in Transwells (membrane pore size, 8 mm; diameter, 6.4 mm; BD Biosciences Discovery Labware) assembled in 24-well plates in 0.1% BSA-RPMI. As a chemoattractant for the cells, the lower chambers were filled up with 10% fetal calf serum-RPMI 1640 medium. Cells were allow migrating for 24 h. The cells that failed to migrate remained on the upper surface and were carefully removed with a cotton swab while cells on the lower surface of the membranes were fixed with 4% PFA and stained with Mayer's hematoxylin (BioOptica, Milan, Italy). Cells were counted under a light microscope at 40× magnification using the new computer-assisted CAST Integrator System (Visiopharm, Hoersholm, Denmark). The average number of cells attached to the lower surface in 30 independent fields (200 mm × 200 mm) per membrane is presented. Each experiment was performed in triplicate.

Western Blot Analysis

A2780 cells were cultivated with an IC_{50} or MC_{50} dose of Sn3 or SBA-15|Sn3 for 6,12, 24 and 48 h and lysed in protein lysis buffer (62.5 mM Tris–HCl (pH 6.8 at 25 ◦C), 2% (w/v) SDS, 10% glycerol, 50 mM dithiothreitol). Electrophoretical separation of proteins was performed on 10–12% SDS-polyacrylamide gels. Electrotransfer to polyvinylidenedifluoride membranes at 5 mA/cm^2 was accomplished with a semidry blotting system (Fastblot B43; BioRad, Göttingen, Germany). Blocking of membranes was done with 5% (w/v) BSA in PBS. Membranes were incubated over night at 4 ◦C with specific antibodies to phospho-Akt,Akt, phospho-p44/p42 MAPK (Erk1/2)(Thr202/Tyr204), p44/p42 MAPK (Erk1/2), phospho-p38 MAPK (Thr180/Tyr182), p38 MAPK, and STAT3 (Cell Signaling Technology, Danvers, MA. USA), and Actin (Abcam, Cambridge, UK). Goat anti-rabbit IgG-HRP (Santa Cruz Biotechnology, Dallas, TX, USA) was used as a secondary antibody. Bands were detected with the chemiluminescence detection system (ECL; GE Healthcare, Chalfont St. Giles, Buckinghamshire, UK).

Results and discussion

Preparation and characterization

The synthesis of $Ph_3Sn(CH_2)_3OH$ (Sn3) as well as SBA-15 and SBA-15p were performed according to the literature procedures.[19,30] SBA-15 was synthesized by sol-gel method and subsequently calcined. SBA-15p was obtained by functionalization of SBA-15 surfaces with 3-chloropropyltriethoxysilane (CPTS), in a subsequent step Sn3 was loaded into SBA-15p (SBA-15|Sn3).

A uniform morphology of MSN particles was observed by SEM and TEM analysis. Thus, images revealed nanostructured-rods shape of the particles with particle size of ca. 670 nm length and ca. 440 nm width (calculated from SEM data) and a uniform pore size with hexagonal distribution (Fig. 1). SEM and TEM images of SBA-15p and SBA-15|Sn3 particles did not demonstrate any substantial alteration to SBA-15 particles indicating that the morphology of the MSNs was not affected after chemical modification (SBA-15p) neither adsorption (SBA-15|Sn3).

The physical parameters of nitrogen adsorption-desorption isotherms, BET surface area, average pore diameter, average pore volume, and wall thickness were measured for all the materials. Thus, nitrogen adsorption-desorption analysis of SBA-15|Sn3 showed a type IV isotherms[36] indicating the mesoporous nature of materials. As expected, the pore diameter as well as surface area of MSNs is affected after subsequent functionalization steps of SBA-15.

View Article Online
DOI: 10.1039/C6DT03519A

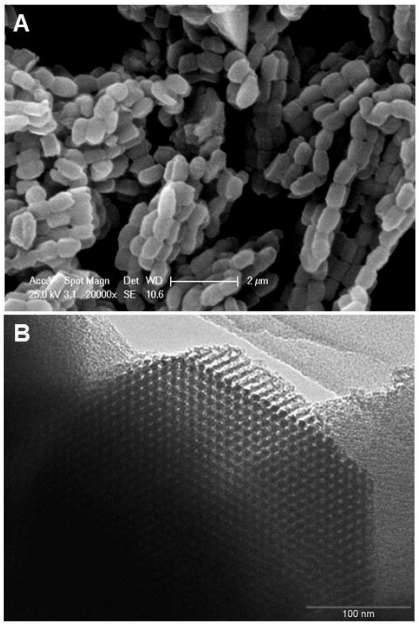

Fig. 1 A. SEM and B. TEM images of SBA-15|Sn3.

Explicitly, uniform pore diameter of 4.97, 4.88 and 4.88 nm, calculated by BJH method,[37] and a high BET surface of 932, 535 and 417 $m^2 \bullet g^{-1}$ (S_{BET}) for SBA-15, SBA-15p and SBA-15|Sn3, respectively, were found. In addition, the wall thickness in materials from SBA-15, SBA-15p to SBA-15|Sn3 (5.68 → 6.03) increased after the first functionalization and remained almost the same (5.82 nm, if not somewhat higher) after the second functionalization.

This indicates that, in the first reaction (with CPTS), the functionalization takes mainly place inside the pore of the nanostructured material, while in the second modification the incorporation of the tin compound may be both in the pore and onto the external surface area.

SBA-15 demonstrated a well-resolved pattern at low 2ϑ values with a very sharp (100) diffraction peak at 0.958. This system can be indexed as a hexagonal lattice with d-spacing values of 92.2. X-ray diffraction pattern (XRD) of the SBA-15p as well as SBA-15|Sn3 materials exhibited also reflections typical for hexagonally ordered mesoporous materials (2ϑ = 0.920 and 0.953; d = 94.8 and 92.7 for SBA-15p and SBA-15|Sn3, respectively).[18] X-ray fluorescence spectroscopy revealed a functionalization rate of 4.35 % (w/w) of Sn per gram of material.

Grafting of SBA-15p was furthermore confirmed by ^{13}C CP/MAS NMR and ^{119}Sn MAS NMR spectroscopy. Additionally to the pattern of the chemical shifts observed in the ^{13}C CP/MAS NMR spectrum of SBA-15|Sn3 appearance of a set of signals related to methylene and phenyl carbon atoms of the Sn3 was detected. In the ^{119}Sn MAS NMR spectrum, a singlet arising from the Sn from tetraorganotin(IV) compound (–105 ppm) corresponds to Sn3 (–99.3 ppm in $CDCl_3$).

Cytotoxicity and mechanism of action of SBA-15|Sn3 against A2780 cell line

The *in vitro* anticancer activity of Sn3, SBA-15p and SBA-15|Sn3 was investigated against ovarian A2780, lung A549 and colon DLD-1 tumor cell lines with SRB assay.[38] The IC_{50} values along with those of cisplatin are presented in Table 2.

Table 2 Cytotoxic potential of Sn3 and SBA-15|Sn3

Compound/Material		A2780	A549	DLD-1
cisplatin	IC_{50} ± SD [μM]	0.6 ± 0.1	1.5 ± 0.1	5.1± 0.2
Sn3		2.8 ± 0.1	3.8 ± 0.1	3.7 ± 0.1
SBA-15|Sn3		2.6 ± 0.5	2.5 ± 0.1	3.5 ± 0.1
SBA-15p	MC_{50} ± SD [μg/mL]	7.2 ± 1.4	6.8 ± 0.1	9.7 ± 0.2
			> 500	

The activity of SBA-15p materials was found inactive under investigated conditions, what is in accordance to previous results.[19] Depending of the cell line Sn3 compound exhibits lower (A2780, A549) or higher activity (DLD-1) than cisplatin. The amount of Sn3 (4.35%) in MC_{50} concentration of SBA-15|Sn3 material is similar to that of IC_{50} dose of free Sn3. However, its activity is in the same concentration range as previously reported analogous MSNs containing hexyl ($Ph_3Sn(CH_2)_6OH$) instead of propyl spacer ($Ph_3Sn(CH_2)_3OH$) in organotin(IV) compound.[19] In addition, activity of SBA-15|Sn3 material is at least 150 times higher than that of the most active titanocene compound, [Ti{Me2Si(η5-C5Me4)(η5-C5H4)}Cl2], grafted into SBA-15 (MC50 = 309±42 μg/mL), from the previous study.[16]

Diminished viability of A2780 cells after exposure to Sn3 or SBA-15|Sn3 was connected with induction of apoptotic cell death. In order to evaluate the apoptotic process, double Ann-PI staining was performed (Fig. 2.A).

Intensified percentage of both early and late apoptotic A2780 cells upon the 72 h of treatment with SBA-15|Sn3 in comparison to Sn3 were detected (Fig. 2.A). Morphological changes of apoptotic cells, such as nuclei shrinkage as well as condensation and/or fragmentation of the DNA, are observed in the A2780 cells treated with Sn3 or SBA-15|Sn3 (Fig. 2.B).

The amount of activated caspases detected was proportional to apoptosis intensity in both cultures (Fig. 2.C). Moreover, it could be clearly observed that activation of caspases initiators 2, 8 and 9 as well as caspase executor 3 upon treatment of A2780 cells occur after 24 h of treatment with free as well as loaded Sn3 compound.

Thus, certain amount of Sn3 is released from nanomaterial, since MSNs are not capable to interact with cell death receptor. In addition to this, analysis of cell cycle distribution (Fig. 2.D) showed accumulation of cells in hypodiploid phase confirming the apoptosis. The presence of cells with fragmented DNA correlated with results of Ann/PI staining. Triggered apoptotic process was well synchronized with enhanced production of ROS species in cell cultures exposed to both free Sn3 and loaded MSN, suggesting their involvement in this process (Fig. 2E).

View Article Online
DOI: 10.1039/C6DT03519A

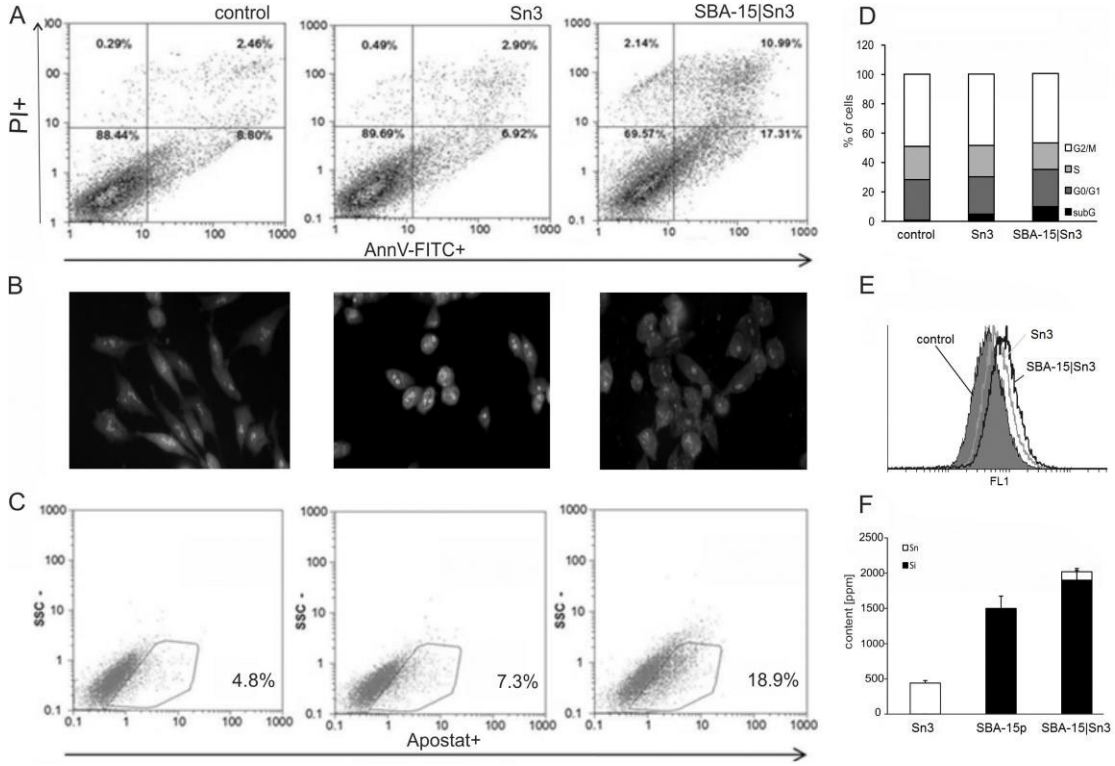

Fig. 2 Sn3 and SBA15|Sn3 induced caspase dependent apoptosis. A) AnnV-FITC/PI double staining; B) AO/EB double staining; C) caspase activation; D) cell cycle distribution; E) ROS induction; D) metal uptake by the cells.

Measurement of intracellular metal amount by ICP-MS after 24 h of cultivation indicated that cells efficiently uptake both Sn3 and SBA-15|Sn3 (Fig. 2.F). However, unexpected ratio of Sn and Si detected in cells treated with nanomaterial SBA-15|Sn3 indicated that drug is released also in extracellular compartment. At least around 30 % of Sn3 found in the cells is not carried by SBA-15p, thus Sn3 enters in the A2780 cells independently. To confirm this findings Sn3 release study from SBA-15|Sn3 in simplified conditions was conducted. Namely, SBA-15|Sn3 was soaked in presence of completed medium in order to obtain desorption behavior of the Sn3 compound (ICP-MS). In concordance with uptake study and caspases activation, the evaluation of Sn3 desorption (see Fig. S7) verified assumption that apart from MSN loaded form, cells are exposed to Sn3 from extracellular compartment that might be related with caspase 8 activation as main sign of receptor dependent apoptosis. Even under this circumstance, previous assessments clearly confirmed that cells acquired enough amount of metal based drug underlining once more that loading into SBA-15p amplified its tumoricidal potential. The response of A2780 cells treated with SBA-15|Sn3 is enhanced in comparison to alone Sn3 notwithstanding 3.7 times lower concentration (ICP-MS) of Sn3.

SBA-15|Sn3 decrease proliferative rate and metastatic properties of A2780 cells

Cells that survived the treatment with Sn3 or SBA-15|Sn3 lost their proliferative potential. Namely, clonogenic survival assay (Fig. 3.A) showed that colony forming potential of cells exposed to Sn3 and especially to SBA-15|Sn3 was dramatically abrogated. Plate efficiency was 34.3; 20.6; 3.1 in control, Sn3 treated and SBA-15|Sn3 treated cells, respectively, with surviving fractions 100; 60; 9. In concordance with this, growth rate of cells pretreated for 72 h with experimental drugs was decreased in comparison to nontreated cells confirming the permanent change of cell phenotype sustained even in the absence of the drug (Fig. 3.B). The cultivation of the cells in 3D cultures on matrigel (Fig. 3.C) was compromised in the presence of Sn3 and dominantly SBA-15|Sn3.

Number, colony form and communication between them was disturbed probably as a consequence of both, decreased dividing potential and mobility of tumor cells. Changed behavior in matrigel was observed in pretreated cultures suggesting that 72 h pulse with the drug is enough for permanent reprogramming of tumor cells. These results have special importance in terms that cultivation in 3D cultures more closely resemble the tumour microenvironment, and therefore are much more relevant for estimation of drugs efficiency.[39]

Simultaneously, affinity of cells to adhere to extracellular matrix was significantly decreased upon exposure to both compound and material (Fig. 3.D). Moreover, the migratory potential of A2780 cells was dramatically affected by tested drugs (Fig. 3.E). According to this, it could be concluded that experimental therapeutics have not just cytotoxic potential but also capacity to suppress their metastatic properties.

View Article Online
DOI: 10.1039/C6DT03519A

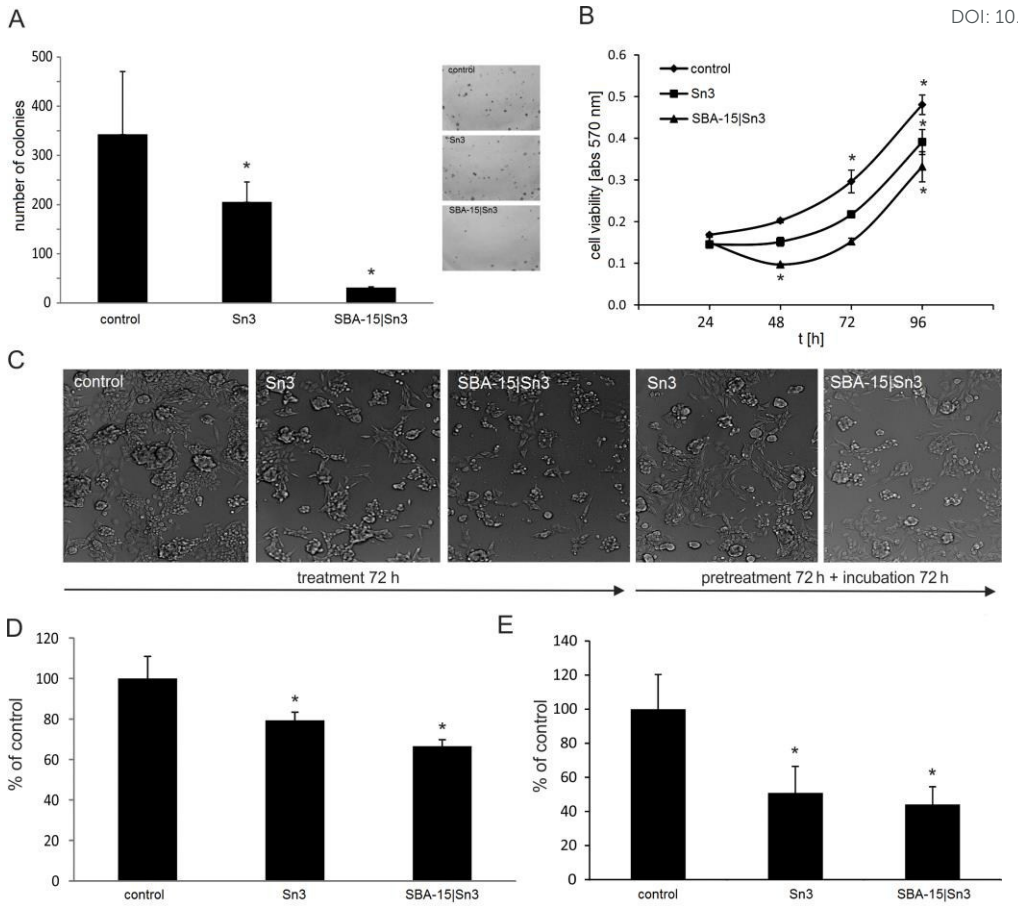

Fig. 3 Sn3 and SBA-15|Sn3 decreased metastatic properties of A2780 cells. A) clonogenic survival assay; B) viability of pretreated cells with Sn3 and SBA-15|Sn3 upon drug removal; C) the growth in 3D cultures; D) adhesion; E) transmigration test.

Difference in the intracellular molecular background of A2780 cells treated with Sn3 and SBA-15|Sn3

To determine drugs influence on the major signaling pathways responsible for cellular proliferation, differentiation and death, Western blot analysis of the expression of p-38, Erk1/2 and Akt has been performed (Fig. 4.A). One of the crucial transcriptional factors regulating the expression of genes involved in growth and apoptosis program in response to different stimuli is STAT3, and therefore its expression was also analyzed.[40] The differences in the expression of Akt and ERK1/2 between Sn3 and SBA-15|Sn3 treated A2780 cells were not observed. While the expression of Akt was transiently suppressed, ERK1/2 phosphorylation was remarkable elevated. Both phenomena are related with the loss of proliferative potential as well as apoptosis induction. Suppression of Akt even in transient mode is basically connected with decreased dividing rate.[41] On the other hand, Erk1/2 activation was observed in numerous cancer cells in response to chemotherapy leading to cell death.[42,43] Interestingly, the expression of p-38 is radically changed after grafting Sn3 in SBA-15p. While its activity is transiently upregulated in cells exposed to Sn3, decreased phosphorylation was detected after treatment with SBA-15|Sn3.

Knowing that activation of the p-38 MAPK pathway plays a role in invasion and metastasis formation, decreased expression of this molecule after SBA-15|Sn3 exposure could be responsible for disturbed matrigel growth, migration and adhesiveness of A2780 cells herein.[44] It is possible that this discrepancy in p-38 regulation contributed to improved potential of Sn3 established upon incorporation to SBA-15p. Similar pattern of changes in STAT-3 expression was noticed. Numerous of data confirming positive relation between STAT3 activity and tumorigenesis as well as tumor progression, bring additional explanation for its improved activity of SBA-15|Sn3 in comparison to naked drug Sn3.

Conclusions

Highly invasive cancers are able to establish resistant phenotype against different chemotherapeutics through multiple mechanism. One of the leading between them is overexpression of MDR pumps. It overcomes efflux of the $Ph_3Sn(CH_2)_3OH$ (Sn3), silica-based nanostructured materials were used as a carrier. Loading of Sn3 into SBA-15p conserved and even potentiated drug effectiveness. Cultivation of cells in the presence of SBA-15|Sn3 led to dual influence of free Sn3 from the extracellular compartment concomitantly with internalized MSN form.

View Article Online
DOI: 10.1039/C6DT03519A

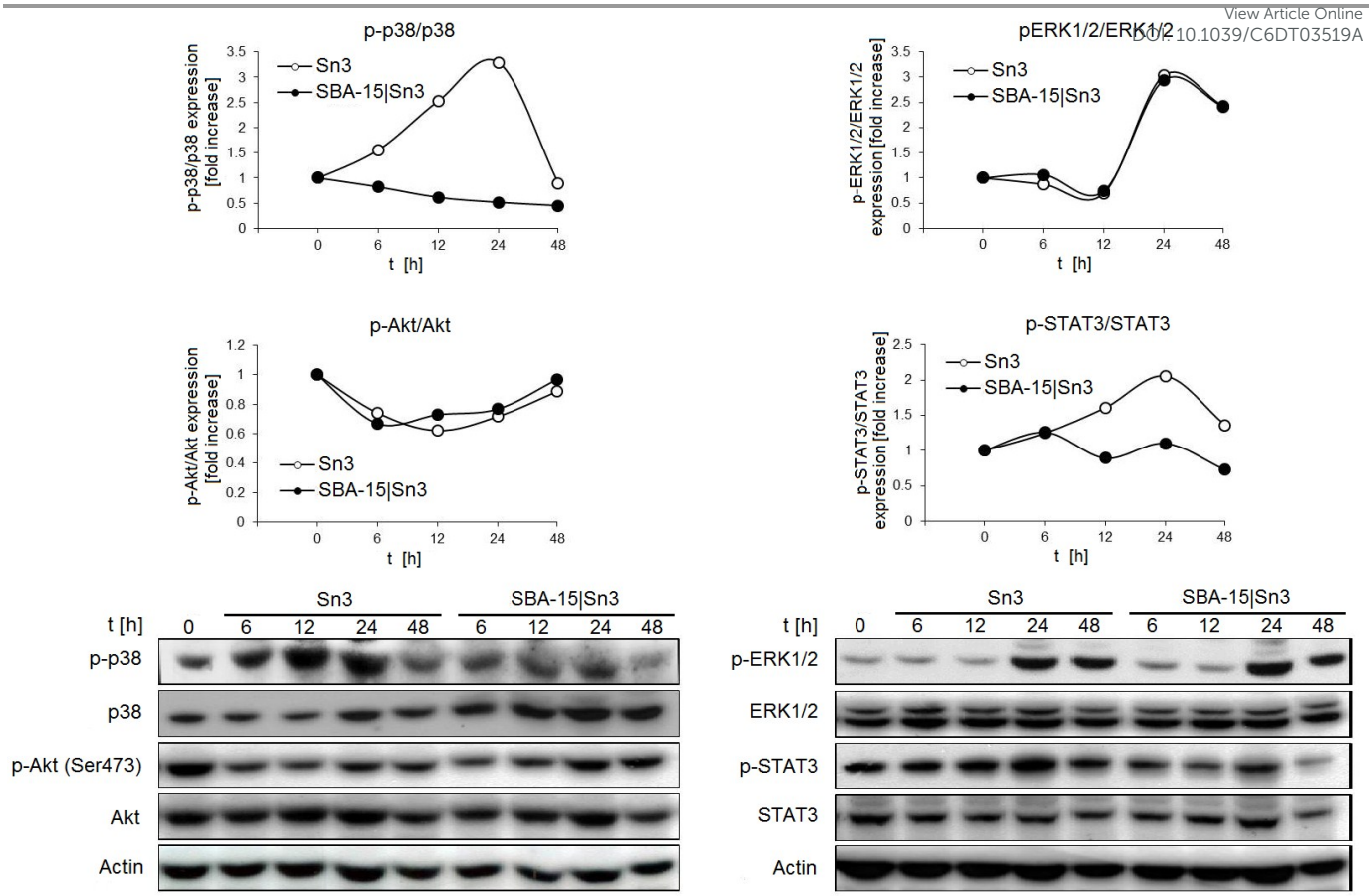

Fig. 4 The influence of Sn3 and SBA-15|Sn3 on the p-38, Akt, Erk1/2 and STAT3 expression.

Antitumor action of SBA-15|Sn3 in A2780 can be ascribed to induction of caspase dependent apoptosis probably triggered by ROS species. In parallel, survived cells displayed changed phenotype with decrease proliferative rate and metastatic properties. Different intracellular molecular background reflected through p-38 and STAT-3 regulation argues better activity of this metal based drug applied in nanocarrier. Taken together, packaging of Sn3 in MSN could be considered as a promising strategy for improvement of chemotherapeutic application.

Conflict of interest

The authors declare no competing financial interest.

Acknowledgments

The authors would like to thank for the support the Serbian Ministry of Education and Science (Grant No 173013), Ministerio de Economía y Competitividad, Spain (Grant no. CTQ2015-66164-R) and Universidad Rey Juan Carlos-Banco de Santander (Excellence Group QUINANOAP).

References

1. A. Baeza, M. Manzano, M. Colilla and M. Vallet-Regí, *Biomater. Sci.*, 2016, **4**, 803–813.
2. J. M. Rosenholm, J. Zhang, M. Linden and C. Sahlgren, *Nanomed.*, 2016, **11**, 391–402.
3. W. A. Wani, S. Prashar, S. Shreaz and S. Gómez-Ruiz, *Coord. Chem. Rev.*, 2016, **312**, 67–98.
4. M. Vallet-Regi, A. Rámila, R. P. del Real and J. Pérez-Pariente, *Chem. Mater.*, 2001, **13**, 308–311.
5. G. S. R. Raju, L. Benton, E. Pavitra and J. S. Yu, *Chem. Commun.*, 2015, **51**, 13248–13259.
6. D. Tarn, C. E. Ashley, M. Xue, E. C. Carnes, J. I. Zink and C. J. Brinker, *Acc. Chem. Res.*, 2013, **46**, 792–801.
7. C.-H. Lu and I. Willner, *Angew. Chem. Int. Ed Engl.*, 2015, **54**, 12212–12235.
8. A. Baeza and M. Vallet-Regí, *Curr. Top. Med. Chem.*, 2015, **15**, 2306–2315.
9. H. Meng, M. Xue, T. Xia, Y.-L. Zhao, F. Tamanoi, J. F. Stoddart, J. I. Zink and A. E. Nel, *J. Am. Chem. Soc.*, 2010, **132**, 12690–12697.
10. B. Rühle, P. Saint-Cricq and J. I. Zink, *Chemphyschem Eur. J. Chem. Phys. Phys. Chem.*, 2016, **17**, 1769–1779.
11. Y. Yang and C. Yu, *Nanomedicine Nanotechnol. Biol. Med.*, 2015, **0**.
12. A. Balbin, F. Gaballo, J. Ceballos-Torres, S. Prashar, M. Fajardo, G. N. Kaluđerović and S. Gómez-Ruiz, *Rsc Adv.*, 2014, **4**, 54775–54787.
13. J. Ceballos-Torres, P. Virag, M. Cenariu, S. Prashar, M. Fajardo, E. Fischer-Fodor and S. Gómez-Ruiz, *Chem. Weinh. Bergstr. Ger.*, 2014, **20**, 10811–10828.

14. Y. Matsumura and H. Maeda, *Cancer Res.*, 1986, **46**, 6387–6392.
15. F. Danhier, O. Feron and V. Préat, *J. Controlled Release*, 2010, **148**, 135–146.
16. D. Perez-Quintanilla, S. Gómez-Ruiz, Z. Zizak, I. Sierra, S. Prashar, I. del Hierro, M. Fajardo, Z. D. Juranic and G. N. Kaluđerović, *Chem.- Eur. J.*, 2009, **15**, 5588–5597.
17. G. N. Kaluđerović, D. Perez-Quintanilla, I. Sierra, S. Prashar, I. del Hierro, Z. Zizak, Z. D. Juranic, M. Fajardo and S. Gómez-Ruiz, *J. Mater. Chem.*, 2010, **20**, 806–814.
18. A. Garcia-Penas, S. Gómez-Ruiz, D. Perez-Quintanilla, R. Paschke, I. Sierra, S. Prashar, I. del Hierro and G. N. Kaluđerović, *J. Inorg. Biochem.*, 2012, **106**, 100–110.
19. M. Z. Bulatovic, D. Maksimovic-Ivanic, C. Bensing, S. Gómez-Ruiz, D. Steinborn, H. Schmidt, M. Mojic, A. Korac, I. Golic, D. Perez-Quintanilla, M. Momcilovic, S. Mijatovic and G. N. Kaluđerović, *Angew. Chem.-Int. Ed.*, 2014, **53**, 5982–5987.
20. Y. Sauntharajah, P. Triozzi, B. Rini, A. Singh, T. Radivoyevitch, M. Sekeres, A. Advani, R. Tiu, F. Reu, M. Kalaycio, E. Copelan, E. Hsi, A. Lichtin and B. Bolwell, *Semin. Oncol.*, 2012, **39**, 97–108.
21. Y. Fan and A. Bergmann, *Trends Cell Biol.*, 2008, **18**, 467–473.
22. A. Jemal, R. Siegel, J. Xu and E. Ward, *CA. Cancer J. Clin.*, 2010, **60**, 277–300.
23. S. Domcke, R. Sinha, D. A. Levine, C. Sander and N. Schultz, *Nat. Commun.*, 2013, **4**, 2126.
24. J. D. Seidman, I. Horkayne-Szakaly, M. Haiba, C. R. Boice, R. J. Kurman and B. M. Ronnett, *Int. J. Gynecol. Pathol. Off. J. Int. Soc. Gynecol. Pathol.*, 2004, **23**, 41–44.
25. D. D. L. Bowtell, *Nat. Rev. Cancer*, 2010, **10**, 803–808.
26. G. E. Konecny, C. Wang, H. Hamidi, B. Winterhoff, K. R. Kalli, J. Dering, C. Ginther, H.-W. Chen, S. Dowdy, W. Cliby, B. Gostout, K. C. Podratz, G. Keeney, H.-J. Wang, L. C. Hartmann, D. J. Slamon and E. L. Goode, *JNCI J. Natl. Cancer Inst.*, 2014, **106**.
27. R. Januchowski, P. Zawierucha, M. Ruciński, M. Andrzejewska, K. Wojtowicz, M. Nowicki and M. Zabel, *Biomed. Pharmacother. Biomed. Pharmacothérapie*, 2014, **68**, 447–453.
28. N. Muhammad and Z. Guo, *Curr. Opin. Chem. Biol.*, 2014, **19**, 144–153.
29. S. Kapse-Mistry, T. Govender, R. Srivastava and M. Yergeri, *Front. Pharmacol.*, 2014, **5**, 159.
30. A. R. Forrester, S. J. Garden, R. A. Howie and J. L. Wardell, *J. Chem. Soc. Dalton Trans.*, 1992, 2615–2621.
31. S. Richter, S. Singh, D. Draca, A. Kate, A. Kumbhar, A. S. Kumbhar, D. Maksimovic-Ivanic, S. Mijatovic, P. Lönnecke and E. Hey-Hawkins, *Dalton Trans. Camb. Engl. 2003*, 2016.
32. G. N. Kaluđerović, V. M. Dinović, Z. D. Juranić, T. P. Stanojković and T. J. Sabo, *J. Inorg. Biochem.*, 2005, **99**, 488–496.
33. M. R. Kaluđerović, G. N. Kaluđerović, S. Gómez-Ruiz, R. Paschke, A. Hemprich, J. Kühling and T. W. Remmerbach, *J. Inorg. Biochem.*, 2011, **105**, 164–170.
34. G. N. Kaluđerović, S. A. Mijatovic, B. B. Zmejkovski, M. Z. Bulatovic, S. Gómez-Ruiz, M. K. Mojic, D. Steinborn, D. M. Miljkovic, H. Schmidt, S. D. Stosic-Grujicic, T. J. Sabo and D. D. Maksimovic-Ivanic, *Metallomics*, 2012, **4**, 979–987.
35. D. Maksimovic-Ivanic, S. Mijatovic, I. Mirkov, S. Stosic-Grujicic, D. Miljkovic, T. J. Sabo, V. Trajkovic and G. N. Kaluđerović, *Metallomics*, 2012, **4**, 1155–1159.
36. K. Sing, D. Everett, R. Haul, L. Moscou, R. Pierotti, J. Rouquerol and T. Siemieniewska, *Pure Appl. Chem.*, 1985, **57**, 603–619.
37. E. P. Barrett, L. G. Joyner and P. P. Halenda, *J. Am. Chem. Soc.*, 1951, **73**, 373–380.
38. W. Voigt, *Methods Mol. Med.*, 2005, **110**, 39–48.
39. H. A. Kenny, M. Lal-Nag, E. A. White, M. Shen, C.-Y. Chiang, A. K. Mitra, Y. Zhang, M. Curtis, E. M. Schryver, S. Bettis, A. Jadhav, M. B. Boxer, Z. Li, M. Ferrer and E. Lengyel, *Nat. Commun.*, 2015, **6**, 6220.
40. K. S. Siveen, S. Sikka, R. Surana, X. Dai, J. Zhang, A. P. Kumar, B. K. H. Tan, G. Sethi and A. Bishayee, *Biochim. Biophys. Acta*, 2014, **1845**, 136–154.
41. J. R. Testa and P. N. Tsichlis, *Oncogene*, 2005, **24**, 7391–7393.
42. 42 S. Cagnol and J.-C. Chambard, *FEBS J.*, 2010, **277**, 2–21.
43. S. Mijatovic, D. Maksimovic-Ivanic, J. Radovic, D. Miljkovic, G. N. Kaluđerović, T. J. Sabo and V. Trajkovic, *Cell. Mol. Life Sci.*, 2005, **62**, 1275–1282.
44. H. K. Koul, M. Pal and S. Koul, *Genes Cancer*, 2013, **4**, 342–359.

View Article Online
DOI: 10.1039/C6DT03519A

A mesoporous silica-based material loaded with organotin compound $Ph_3Sn(CH_2)_3OH$ diminished metastatic properties of A2780 survived cells.